Proc. of SPIE Vol. 3056, Thermosense XIX: An International Conference on Thermal Sensing and Imaging Diagnostic Applications, ed. R N Wurzbach, D D Burleigh (Apr 1997) Copyright SPIE

# Visualization of Contact Stress Distribution Using Infrared Stress Measurement System

Takahide SAKAGAMI[a], Keiji OGURA[b], Shiro KUBO[a], Jon R. LESNIAK[c], Bradley R. BOYCE[c] and Bela I. SANDOR[d]

[a] Faculty of Engineering, Osaka University, 2-1, Yamadaoka, Suita, Osaka 565 Japan

[b] Faculty of Engineering Science, Osaka University, Toyonaka, Osaka 560 Japan

[c] Stress Photonics Inc., 3002 Progress Road, Madison WI 53716 U.S.A.

[d] University of Wisconsin-Madison, 1500 Engineering Drive, Madison WI 53706 U.S.A.

## Abstract

A new experimental technique using an infrared stress measurement system and an infrared transmitting material is proposed for the visualization of a contact stress distribution. An infrared transmitting material is employed as one of two contacting materials, and is brought into contact with a cyclically loaded sample. Infrared emissions from the contact surface are measured through the infrared transmitting material, and thermoelastic stress analysis (TSA) is applied to measure the contact stress distribution. First, a flat contact is investigated, in which a barium-fluoride window is in contact with an embossed plastic letter. Stress distribution on the contact area in the letter can be measured accurately. Further, a spherical Hertz contact is examined by using an infrared transmitting sapphire convex lens and a flat plastic plate. The obtained contact stress distribution is compared with the stress distribution predicted by the Hertz theory. An excellent correspondence is found between those stress distributions, indicating the feasibility of quantitative analysis using the present technique.

Keywords : Infrared stress measurement, Thermoelastic effect, Contact stress, Infrared transmitting material, Hertz contact, Tribology

## 1. Introduction

Investigation of tribological phenomena such as friction, lubrication, wear and fretting fatigue is important in many fields of science and engineering. Recently, the importance of tribological studies has been widely recognized in reliability evaluations not only for machine and structural components but also for artificial joints used in human bodies. Contact stress measurement is one of the indispensable subjects in the investigation of tribological phenomena.

Analytical solutions, including Hertz theory for contact problems [1], have been widely used for investigating contact stress distribution. They give an accurate stress distribution under the ideal contact between two solids with simple shapes, such as for a flat surface touching a spherical surface. In actual engineering applications, however, the contact is usually more complicated, since it is affected by the shape and roughness of the contact surface as well as material properties. Thus development of a practical method for evaluating the contact stress distribution is required in many fields.

Recently a numerical approach combined with an inverse analysis has been successfully applied to contact stress evaluation, in which the stress distribution on the contact surface is estimated from stress values measured on other portions of the body. Oda et al. [2] proposed an inverse analysis technique for identifying a contact stress distribution. Kubo et al [3] also developed a finite element-based inverse analysis scheme for estimating distributions of tractions and displacements on the contact surface.

Direct experimental investigation of contact stress distribution has not been done in prior research. Only pressure sensitive paint or contact pressure sensors have been used for the crude measurement of macroscopic contact pressure distribution.

For the direct observation of the contact surface, a new infrared thermography technique combined with infrared transmitting materials was proposed by some of the present authors [4,5]. An infrared transmitting material, such as sapphire or fluorides, was used as one of the two contact solids. The contact surface was observed by infrared thermography through

the infrared transmitting solid. This technique was successfully employed for dry sliding contact temperature measurements and for the direct observation of dynamic wear processes.

In this paper, this technique is applied to the visualization of contact stress distribution between an infrared transmitting solid and a sample material by using an infrared stress measurement system based on thermoelastic stress analysis (TSA). First, the contact stress resulting from a flat contact is examined, by putting a barium-fluoride window in contact with an embossed plastic typeface. Next, a spherical Hertz contact is examined for several kinds of plastic plate samples using a sapphire convex lens as an infrared transmitting material.

## 2. Experimental Technique for Contact Stress Measurement

### 2.1 Thermoelastic stress analysis (TSA)

All materials, whether solid, liquid or gas, change temperature when they are compressed or expanded. In solids dynamic stress changes cause small temperature changes. This phenomenon is known as the thermoelastic effect and is described by the thermoelastic equation that relates temperature change ($\Delta T$) to a change in the sum of the principal stresses ($\Delta\sigma$) under cyclic loading.

$$\Delta T = -\frac{\alpha T}{\rho C_p}\Delta\sigma \tag{1}$$

$\alpha$ = coefficient of thermal expansion
$\rho$ = mass density
$C_p$ = specific heat at constant pressure
$T$ = absolute temperature

For TSA, a differential thermography system of less than 5mK resolution is needed. Such a system correlates the load-induced infrared signal with the reference loading signal enabling the measurement of very small temperature changes due to the thermoelastic effect.

### 2.2 Infrared transmitting solid

Typical infrared sensor employed in differential thermography systems are sensitive in wavelength regions of either 3-5μm or 8-12μm. Several kinds of optical solids shown in Table 1, which have transmission range over such wavelengths, have been employed for the window materials.

Table 1 IR transmitting materials.

| | Material | Transmittance (%) | Hardness |
|---|---|---|---|
| Medium Wave IR (3~5μm) | Si | 55* | Hk=1150 (P=500g) |
| | Alumina | 70~80 | Hv=2100 |
| | Sapphire | 70~85 | Hk=1700 (P=500g) |
| | $MgF_2$ | 95 | Hk=415 (P=500g) |
| | $CaF_2$ | 95 | Hk=158 (P=500g) |
| Medium and Long Wave IR (3~5, 8~12μm) | Ge | 45* | Hk=190 (P=50g) |
| | $BaF_2$ | 95 | Hk=82 (P=500g) |
| | ZnS | 60~75 | Hk=160 (P=50g) |
| | ZnSe | 75 | Hk=105 (P=50g) |

* without anti reflection coating

### 2.3 Contact stress measurement using infrared transmitting solid

Consider a contact situation shown in Fig.1. A ball is in contact with an infrared transmitting disk. Cyclic compressive load is applied to the ball. The contact surface is observed from the disk side by the differential thermography

camera. The thermoelastic temperature change due to the cyclic stress on the contact surface of the ball can be measured by differential thermography, since the infrared emission from the contact surface passes through the infrared transmitting disk with minimal absorption and scatter. This enables us to measure contact stresses using TSA.

## 2.4 Experimental system

The testing apparatus used for the contact stress measurement is shown schematically in Fig. 2. For example, a test sample on the loading stage was brought into contact with an infrared transmitting convex lens and was cyclically loaded by the electro-dynamic shaker. A load signal was monitored by a load cell and was employed as the reference signal of the differential thermography system. The dynamic temperature change due to the contact stress was measured by TSA through the infrared transmitting material. The contact stress, i.e., the range in the sum of the principal stresses was determined from the thermoelastic equation [Eq.(1)].

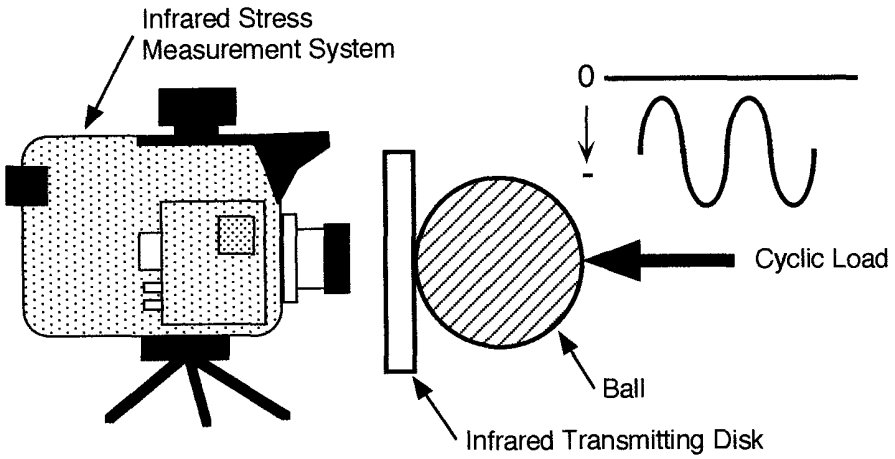


Fig. 1 Contact stress measurement based on the infrared emission from the contact surface due to the thermoelastic effect.

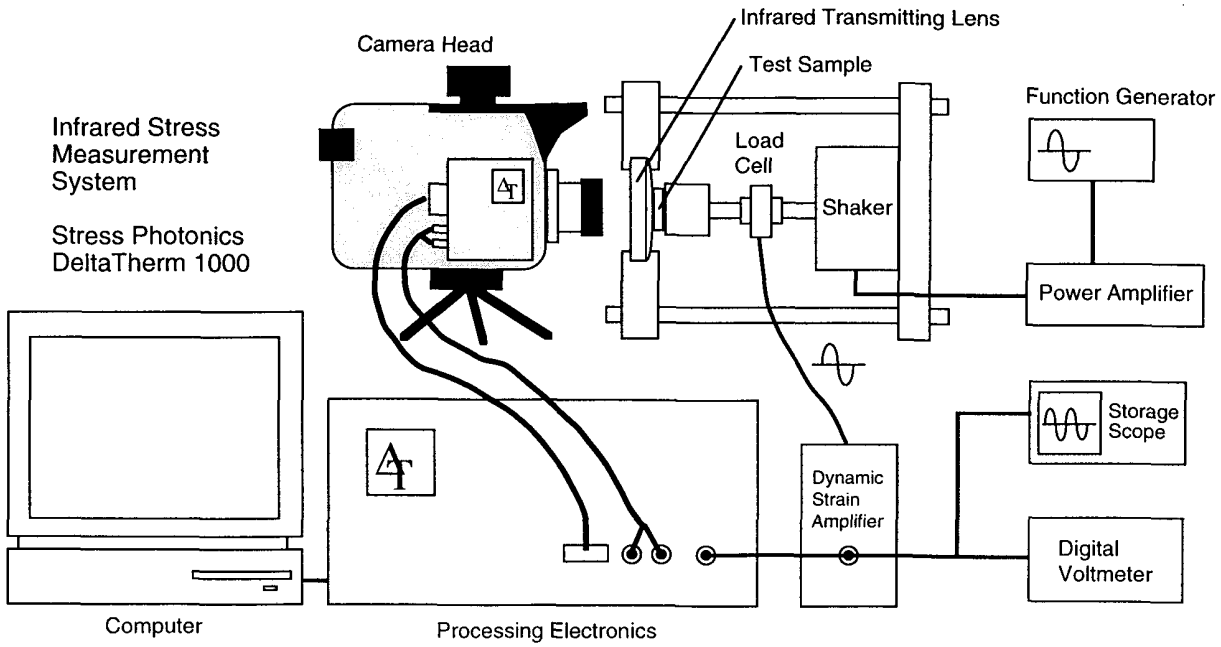


Fig. 2 Schematic illustration of the apparatus used for the contact stress measurement.

Table 2 Specifications of the differential thermography system.

| | |
|---|---|
| Detector | InSb 128x128 Elements Array |
| Spectral Range | 3-5 μm |
| Frequency Range of Reference Signal | 1Hz - 1kHz |
| Frame Rate | 434 frames/s |
| Thermal Resolution | 2mK (30s acquisition time, 1-160Hz) |

The specifications of the differential thermography system are shown in Table 2. A spacer ring for magnification was mounted between the infrared array detector and the infrared camera lens for the measurement of the stress distribution in a small area. The imaging area was 8.7mm square and the spatial resolution of the stress measurement was 70μm.

Sapphire and Barium-fluoride ($BaF_2$) were chosen because they both transmit infrared well in the 3-5μm range, and because of their hardness (sapphire in particular). These window materials were used because of the InSb infrared sensor in the thermography system.

## 3. Stress Measurements in Flat Contact

### 3.1 Testing Conditions

First, flat-contact stresses, where the size of the contact area is kept constant in the cyclic loading, were examined to confirm the feasibility of the proposed method.

A pair of plastic embossed letters was the specimen for the flat contact experiment. Dimensions of the specimen are shown in Fig. 3. The surface of the letters was coated with a flat black paint to prevent reflection at the contact surface.

The plastic letters were fixed on the loading stage and were brought into contact with a $BaF_2$ disk. Cyclic compressive loads were applied to the test sample in two different loading conditions shown in Table 3. The stress distribution on the contact surface of the letters was measured by the thermography system.

### 3.2 Experimental results

Contact stress images represented by the infrared signal intensity $\Delta V$ were obtained for different loading conditions shown in Fig. 4. The stressed area on the contact surface of the characters "S" and "P" were clearly identified in the images taken by the present system. The absolute values of the measured infrared signal were proportional to the amplitude of the cyclic compressive load.

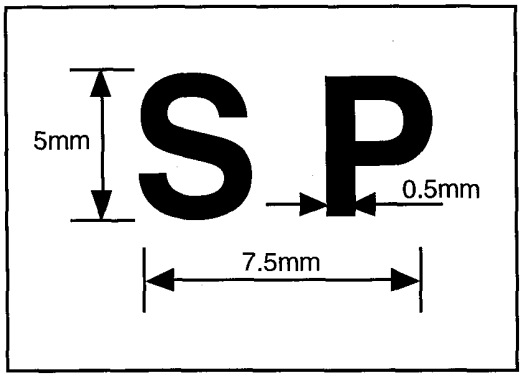


Fig. 3 Dimensions of the embossed letter specimen.

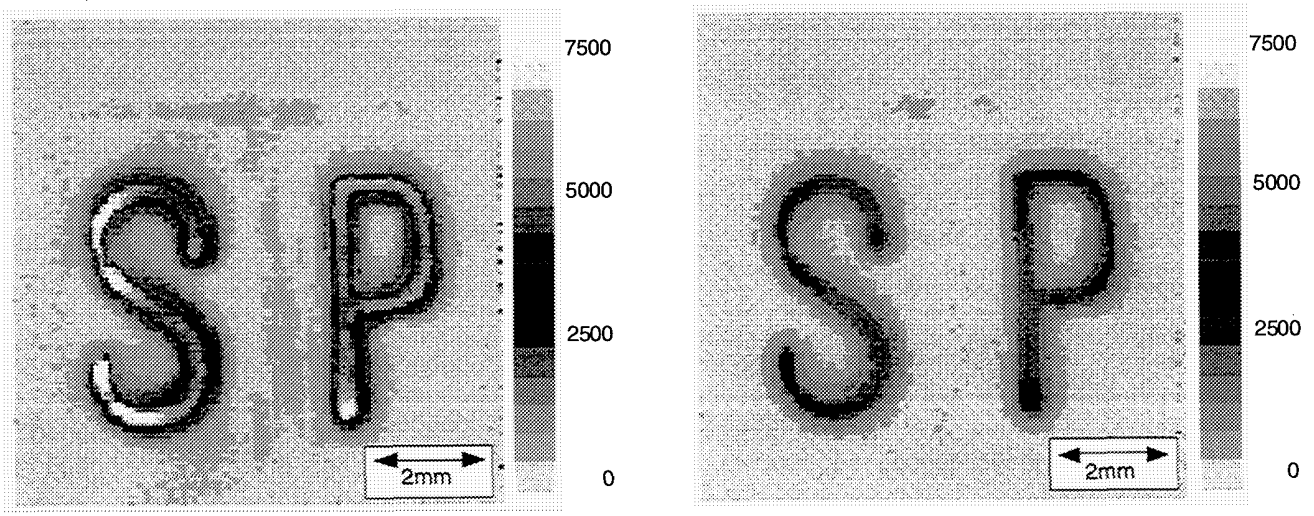


(a) Exp-1 $P$=11.45±6.26 (N)　　(b) Exp-2 $P$=11.96±3.10 (N)

Fig. 4 Images of the contact stress distribution on embossed letters obtained by the infrared stress measurement system.
(See color plate p. 259)

Table 3 Applied cyclic load in flat contact.

| Exp. No. | Applied Load P (N) | Frequency(Hz) |
|---|---|---|
| Exp-1 | 11.45±6.26 | 45 |
| Exp-2 | 11.96±3.10 | 45 |

## 4. Stress Measurements in Spherical Hertz Contact

### 4.1 Testing apparatus and loading conditions

Stresses caused by spherical Hertz contact were measured for several plastics as shown in Table 4. A flat plate sample (15mm×15mm, 1.6mm in thickness) was mounted on the loading stage and was brought into contact with a sapphire convex lens that has a spherical contact surface with a radius of curvature of 150mm. Sand blasting was done on the contact surface of the plastic sample to prevent reflections and to obtain a high emissivity. Cyclic compressive loads were applied in several combinations of mean and amplitude values of compressive load and at various frequencies. In this paper, the polypropylene (material A) and the polycarbonate (material E) are selected and the experimental results obtained for three loading conditions as shown in Table 5 are examined.

Table 4 Plastics used for contact stress measurement.

| | |
|---|---|
| material A | Polypropylene |
| material B | ABS resin |
| material C | Polyethylene |
| material D | Acryl |
| material E | Polycarbonate |
| material F | Nylon 66 |
| material G | Delrin |

Table 5 Loading conditions and ranges in sums of principal stresses obtained by the Hertz theory.

| Sample A7 (Polypropylene) | | | | | | |
|---|---|---|---|---|---|---|
| Exp. No. | Applied Load P (N) | Frequency (Hz) | $a_{min}$ (mm) | $a_{max}$ (mm) | $\Delta\sigma_{max}$ (MPa) | $\Delta\sigma_0$ (MPa) |
| A7-09 | 29.0±11.8 | 45 | 1.56 | 1.17 | 14.1 | 5.4 |
| A7-11 | 29.0±19.9 | 45 | 1.65 | 0.95 | 18.6 | 9.7 |
| A7-19 | 45.8±11.7 | 45 | 1.75 | 1.47 | 12.9 | 3.8 |
| Sample E8 (Polycarbonate) | | | | | | |
| Exp. No. | Applied Load P (N) | Frequency (Hz) | $a_{min}$ (mm) | $a_{max}$ (mm) | $\Delta\sigma_{max}$ (MPa) | $\Delta\sigma_0$ (MPa) |
| E8-09 | 29.4±11.7 | 45 | 1.26 | 0.95 | 21.7 | 8.1 |
| E8-11 | 29.5±19.8 | 45 | 1.33 | 0.78 | 28.5 | 14.7 |
| E8-19 | 46.0±11.8 | 45 | 1.41 | 1.18 | 19.8 | 5.8 |

## 4.2 Hertz theory

Theoretical analyses for the contact area and contact stress distribution were done based on the Hertz theory for the spherical contact.

At the maximum compressive load in the cycle, the radius of the contact area $a_{max}$ and the contact pressure $p_{max}$ are given by the following equations.

$$a_{max} = \sqrt[3]{\frac{3}{4} P_{max} R \left( \frac{1-\nu_1^2}{E_1} + \frac{1-\nu_2^2}{E_2} \right)} \tag{2}$$

$$p_{0max} = \frac{3P_{max}}{2\pi a_{max}^2}, \qquad p_{max} = p_{0max} \sqrt{1 - \frac{r^2}{a_{max}^2}} \tag{3}$$

where $E_1$, $\nu_1$ and $E_2$, $\nu_2$ are Young's modulus and Poisson's ratio for the plastic sample and the sapphire lens, respectively. $R$ is the radius of curvature of the lens, and $r$ is the distance from the center of the circular contact area where the maximum contact pressure $p_{omax}$ is given. In the same way, the radius of the contact area $a_{min}$ and the contact pressure $p_{min}$ at the minimum compressive load are given by the following equations.

$$a_{min} = \sqrt[3]{\frac{3}{4} P_{min} R \left( \frac{1-\nu_1^2}{E_1} + \frac{1-\nu_2^2}{E_2} \right)} \tag{4}$$

$$p_{0min} = \frac{3P_{min}}{2\pi a_{min}^2}, \qquad p_{min} = p_{0min} \sqrt{1 - \frac{r^2}{a_{min}^2}} \tag{5}$$

Material properties needed in the analyses are given in Table 6.

Stress components in the cylindrical coordinates $\sigma_r$, $\sigma_\theta$ and $\sigma_z$ can be calculated from the contact pressure distribution, and the range in the sum of the principal stresses ($\Delta\sigma$) is given by the following equation.

$$\Delta\sigma = 2(1+\nu)(p_{max} - p_{min}) \tag{6}$$

Table 6 Material properties.

| Material | Young's Modulus E (GPa) | Poisson's Ratio ν |
|---|---|---|
| Polypropylene (A) | 1.088 | 0.33 |
| Polycarbonate (E) | 2.089 | 0.33 |
| Sapphire | 335.0 | 0.25 |

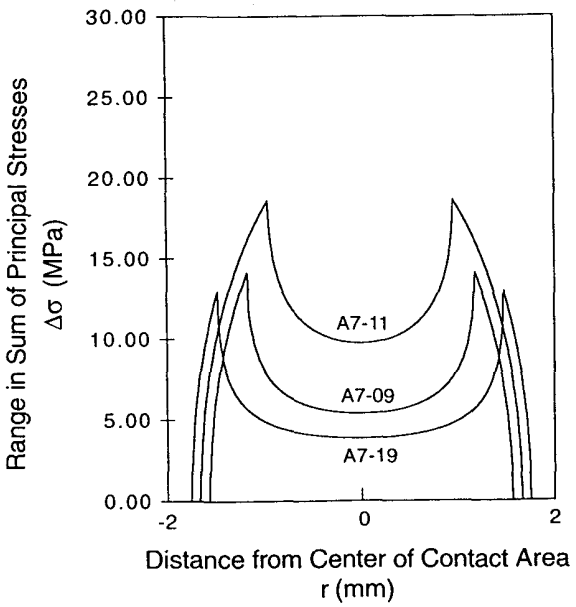


Fig. 5 Distribution of the range in the sum of the principal stresses obtained by the Hertz theory for polypropylene sample.

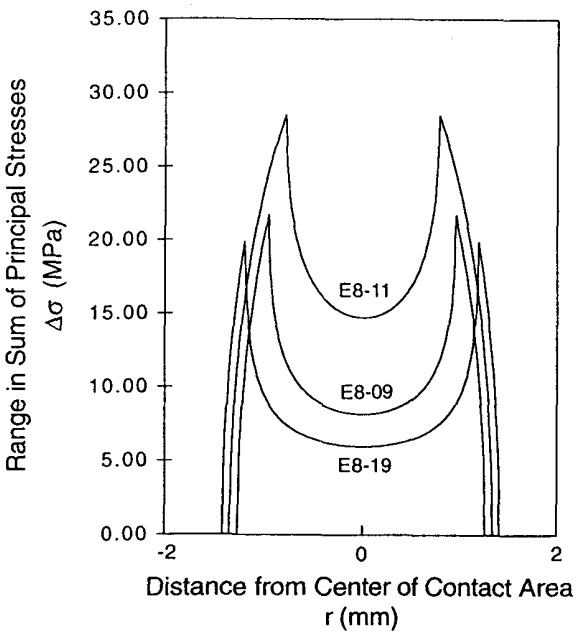


Fig. 6 Distribution of the range in the sum of the principal stresses obtained by the Hertz theory for polycarbonate sample.

Distributions of $\Delta\sigma$ were calculated by the Hertz theory for the test conditions shown in Table 5, and plotted in Figs. 5 and 6 for the polypropylene sample and the polycarbonate sample, respectively. It is found that $\Delta\sigma$ shows an axisymmetric distribution, where $\Delta\sigma$ is increasing from its central value $\Delta\sigma_0$ up to the maximum value $\Delta\sigma_{max}$ at $r=a_{min}$, then $\Delta\sigma$ is decreasing to zero at $r=a_{max}$. Theoretical values of $a_{min}$, $a_{max}$, $\Delta\sigma_0$ and $\Delta\sigma_{max}$ obtained for each experiment are shown in Table 5.

### 4.3 Experimental results of contact stress measurement

The contact stress distributions measured as the distribution of the intensity $\Delta V$ of infrared emission from the contact surface due to the thermoelastic effect are shown in Figs. 7 and 8 for polypropylene and polycarbonate, respectively. The circles indicating the maximum and minimum contact areas are also shown in the figures. Line profiles obtained along the lines x-x in Fig. 7 are plotted in Fig. 9. An excellent correspondence is found between the contact stress distributions measured by the infrared system and those obtained by the Hertz theory. $\Delta V$ is increasing from the center of the contact area up to the maximum value at $r=a_{min}$, then $\Delta V$ is decreasing to near zero at $r=a_{max}$. And smaller contact area at each load was observed for the polycarbonate sample that has a larger Young's modulus than that of polypropylene. Figs. 5 and 9 show that a comparison for the magnitude of $\Delta\sigma$ can be made among different loading conditions. The unsymmetric peaks in Fig. 9 are probably caused by inhomogeneous geometries of the surfaces in contact.

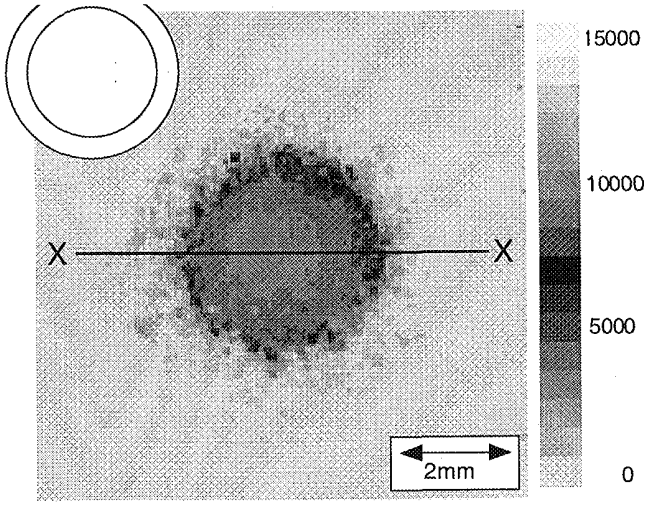


(a) A7-09 P = 29.0 ± 11.8 (N)

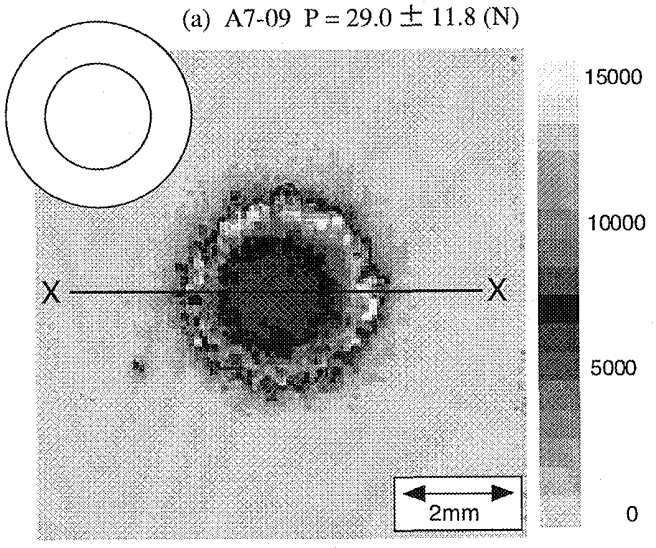


(b) A7-11 P = 29.0 ± 19.9 (N)

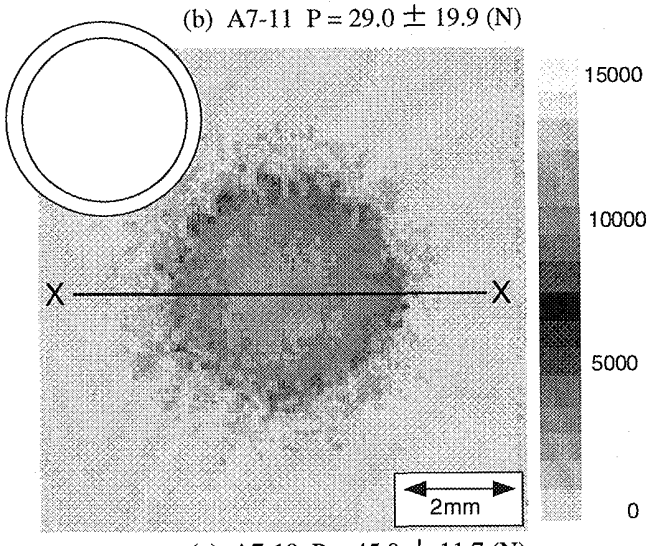


(c) A7-19 P = 45.8 ± 11.7 (N)

Fig. 7 Images of contact stress distributions for the Hertz contact between polypropylene sheet and sapphire convex lens obtained by the infrared stress measurement system.

(See color plate p. 259)

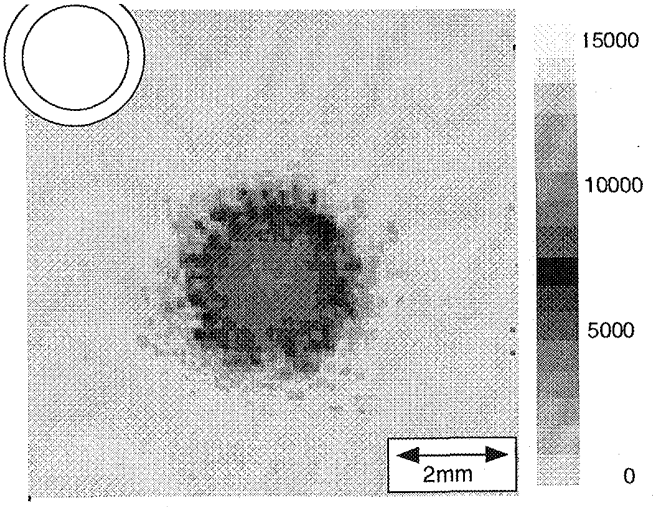


(a) E8-09 P = 29.4 ± 11.8 (N)

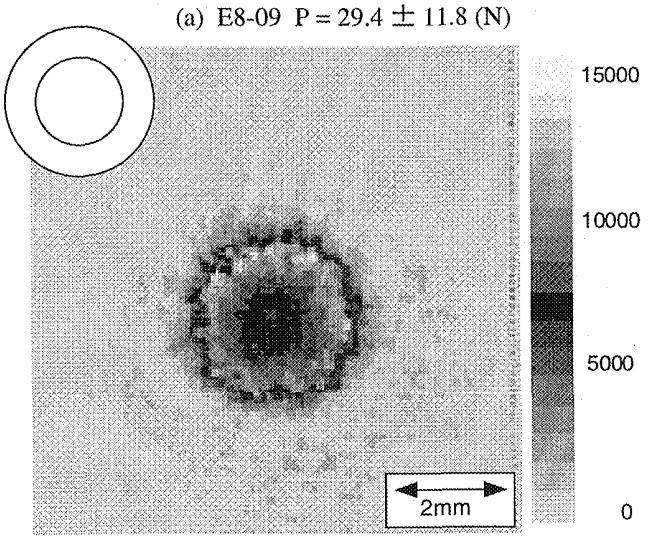


(b) E8-11 P = 29.4 ± 19.9 (N)

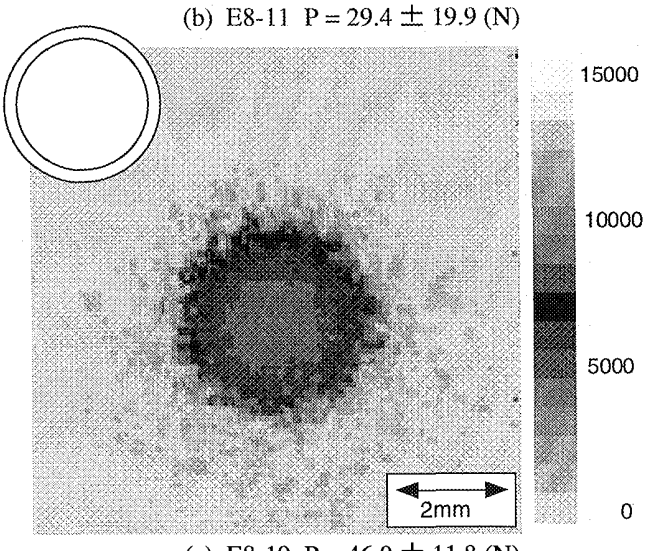


(c) E8-19 P = 46.0 ± 11.8 (N)

Fig. 8 Images of contact stress distributions for the Hertz contact between polycarbonate sheet and sapphire convex lens obtained by the infrared stress measurement system.

(See color plate p. 259)

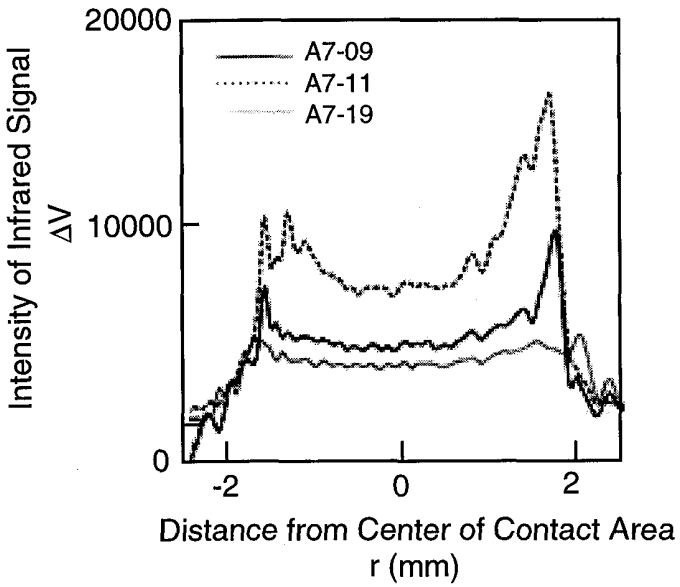


Fig. 9 Distribution of the intensity DV of infrared emission along lines X-X in Fig. 7.

## 5. Conclusions

A new experimental technique using an infrared stress measurement system and an infrared transmitting material was proposed for the visualization of a contact stress distribution. Stress distribution on the contact surface was examined for a flat contact as well as for a spherical Hertz contact. It was found that contact stress distribution can be determined quantitatively. Calibrations will be needed to obtain absolute values of contact stresses. The calibrations should involve reliable values of the thermal conduction from the plastic sample to the sapphire lens, the infrared transmittance in the sapphire lens, and the thermoelastic constant of the plastic sample.

## Acknowledgement

This research was partially supported by the Visiting Scholar Program of the Japan Ministry of Education, Science, Sports and Culture.

## References

(1) K.L.Johnson, Contact Mechanics, (1985), Cambridge University Press.
(2) J.Oda and T.Shinada, On Inverse Analysis Technique to Obtain Contact Stress Distributions, Trans. of JSME, Ser. A, 53-492, (1987), pp.1614-1620.
(3) S.Kubo, K.Ohji, and T.Ueda, A Finite Element-Based Inverse Analysis Scheme Using Function Expansion for Estimating Distributions of Tractions and Displacements on Contact Area, Extended Abstract of the 3rd World Congress on Computational Mechanics, Vol.II, (1994), pp.972-973
(4) T.Sakagami, K.Ogura and M.Shoda, Thermal Sensing and Imaging of the Dry Sliding Contact Surface Using IR Thermo-Microscope, SPIE Proceedings Series Volume 2473, (1995), pp.263-272.
(5) T.Sakagami and K.Ogura, Applications of Infrared Thermography in Contact Mechanics, Proc. of Conference on Advanced Technology in Experimental Mechanics, (1995), pp.229-233.

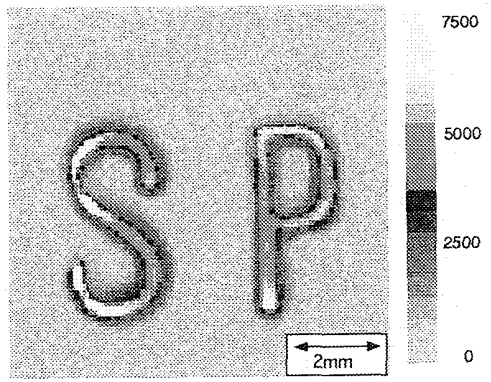


(a) Exp-1 $P$=11.45±6.26 (N)

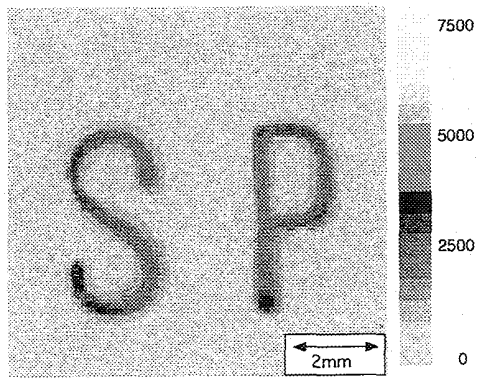


(b) Exp-2 $P$=11.96±3.10 (N)

Fig. 4 Images of the contact stress distribution on embossed letters obtained by the infrared stress measurement system.

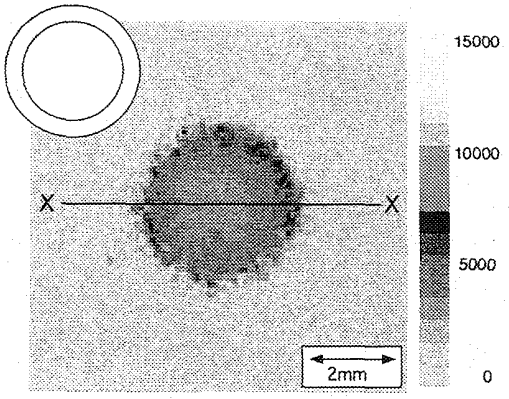


(a) A7-09 P = 29.0 ± 11.8 (N)

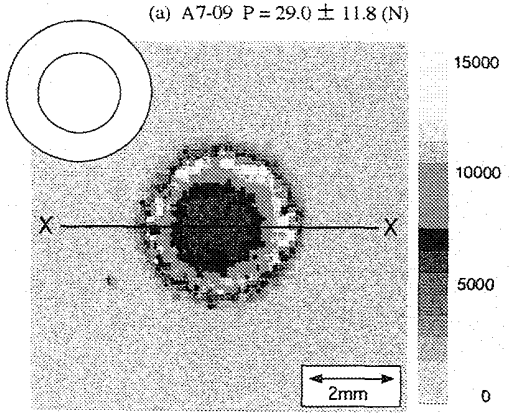


(b) A7-11 P = 29.0 ± 19.9 (N)

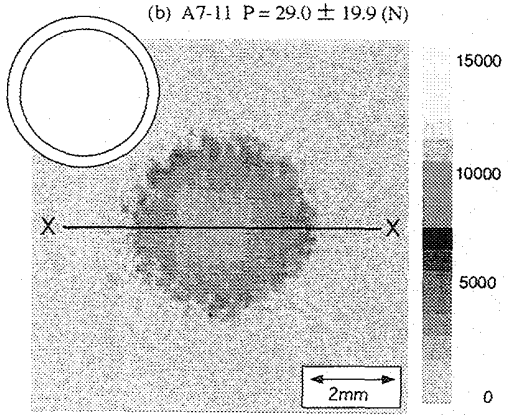


(c) A7-19 P = 45.8 ± 11.7 (N)

Fig. 7 Images of contact stress distributions for the Hertz contact between polypropylene sheet and sapphire convex lens obtained by the infrared stress measurement system.

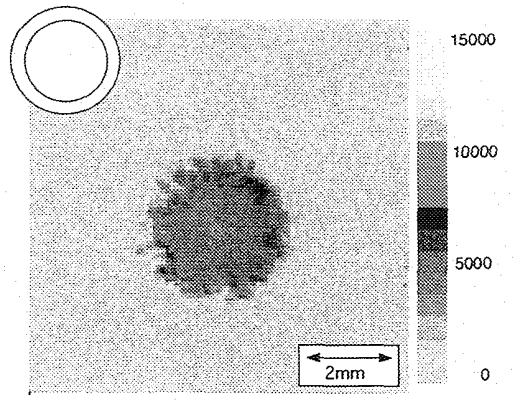


(a) E8-09 P = 29.4 ± 11.8 (N)

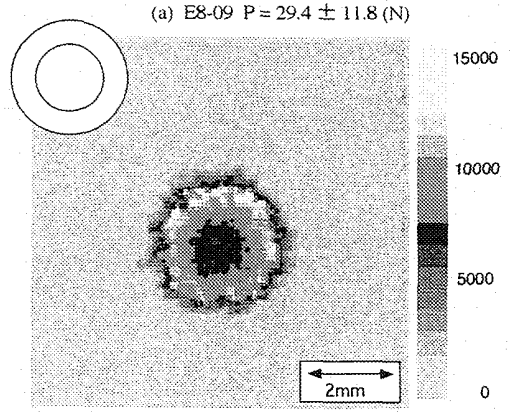


(b) E8-11 P = 29.4 ± 19.9 (N)

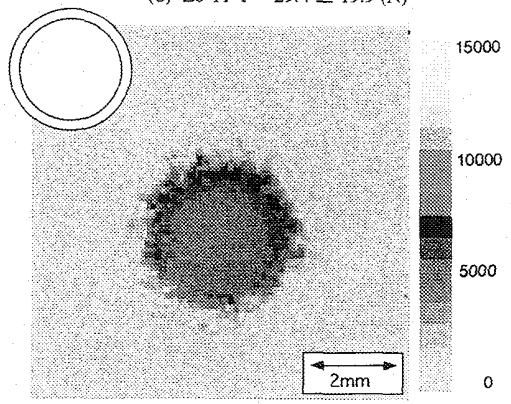


(c) E8-19 P = 46.0 ± 11.8 (N)

Fig. 8 Images of contact stress distributions for the Hertz contact between polycarbonate sheet and sapphire convex lens obtained by the infrared stress measurement system.



259